Magnetic Resonance Materials in Physics, Biology and Medicine
https://doi.org/10.1007/s10334-018-0673-0

RESEARCH ARTICLE

Influence of principal component analysis acceleration factor on velocity measurement in 2D and 4D PC-MRI

Gwenaël Pagé[1] · Jérémie Bettoni[2] · Anne-Virginie Salsac[3] · Olivier Balédent[1,4]

Received: 15 September 2017 / Revised: 28 December 2017 / Accepted: 3 January 2018

Abstract

Objective The objective of the study was to determine how to optimize 2D and 4D phase-contrast magnetic resonance imaging (PC-MRI) acquisitions to acquire flow velocities in millimetric vessels. In particular, we search for the best compromise between acquisition time and accuracy and assess the influence of the principal component analysis (PCA).

Materials and methods 2D and 4D PC-MRI measurements are conducted within two in vitro vessel phantoms: a Y-bifurcation phantom, the branches of which range from 2 to 5 mm in diameter, and a physiological subject-specific phantom of the carotid bifurcation. The same sequences are applied in vivo in carotid vasculature.

Results For a vessel oriented in the axial direction, both 2D and axial 4D PC-MRI provided accuracy measurements regardless of the *k-t* PCA factor, while the acquisition time is reduced by a factor 6 for *k-t* PCA maximum value. The in vivo measurements show that the proposed sequences are adequate to acquire 2D and 4D velocity fields in millimetric vessels and with clinically realistic time durations.

Conclusion The study shows the feasibility of conducting fast, high-resolution PC-MRI flow measurements in millimetric vessels and that it is worth maximizing the *k-t* PCA factor to reduce the acquisition time in the case of 2D and 4D axial acquisitions.

Keywords Cine MRI · Principal component analysis · Feasibility studies · Imaging phantoms

Introduction

Phase-contrast magnetic resonance imaging (PC-MRI) is a noninvasive technique used to quantify and characterize blood flow [1, 2]. Over the years, it has progressed from 2D acquisitions of the flow velocity along one direction in space for an individual slice, to 3D velocity measurement within an acquired volume [3, 4]. The latter is classically referred to as 4D, with reference to the three spatial dimensions plus time. Four-dimensional PC-MRI is increasingly being used in clinical practice to characterize blood flow in large arteries and within the heart [5, 6]. By providing patient-specific measurements of the hemodynamic conditions, it is used to diagnose and plan treatment for vascular diseases, such as aortic coarctations and aneurysms [7, 8]. It is also used to assess quantities such as wall shear stresses (WSS) [9, 10] and mechanical properties of arterial walls, one technique consisting of measuring the pulse wave velocity in the vessel of interest [11].

One limitation of 4D PC-MRI is its ability to accurately determine flow fields in vessels < 1 cm in diameter, the limiting factors being spatial resolution and acquisition time length. Recent publications have demonstrated the advantages of PC-MRI to study hemodynamics in smaller vessels, such as intracranial vessels [12–14]—for instance, to manage intracranial aneurysms [15]. However, few measurements have been acquired using 4D PC-MRI because of

✉ Gwenaël Pagé
gwenael.page@hotmail.fr

Olivier Balédent
olivier.baledent@chu-amiens.fr

1 BioFlow Image, University Hospital of Amiens Picardy, Université de Picardie Jules Verne, Avenue Rene Laennec, Salouël, 80480 Amiens, France

2 Maxillo-Facial Surgery, University Hospital of Amiens-Picardie, Amiens, France

3 Biomechanics and Bioengineering Laboratory (UMR CNRS 7338), Sorbonne Universités, Université de Technologie de Compiègne–CNRS, Compiègne, France

4 Laboratory of Image Processing, University Hospital of Amiens-Picardie, Amiens, France

Published online: 22 January 2018

spatial resolution that is too low and acquisition times too long for in-patient measurement. Four-dimensional PC-MRI would provide more complete information on the velocity field than classical 2D acquisitions, as it enables reconstruction of flow streamlines within vessels and assesses all components of the WSS tensor [5, 16].

Despite constraints of signal-to-noise ratio (SNR) and spatial resolution, some studies have conducted 4D PC-MRI sequences on head and neck arteries. Harloff et al. [17] acquired blood flow velocities in carotid arteries with a pixel resolution of $1.1 \times 0.9 \times 1.4$ mm^3 for a total scanning time of 15–20 min. They compared their results with Doppler ultrasound (US) measurements, which indicated that the 4D PC-MRI technique is promising to visualize vector fields. Markl et al. [18] performed 4D PC-MRI acquisitions in carotid arteries with a voxel size of $1.1 \times 0.9 \times 1.4$ mm^3 to estimate WSS. In both studies, higher spatial resolution would have been needed to accurately analyze the flow inside vessels and determine WSS. It would, however, have generated acquisition times incompatible with clinical practice. One possibility of increasing spatial resolution while keeping a good SNR is to use a dStream (dS) Microscopy MRI coil. It is designed for measurements in superficial vessels and is characterized by a higher SNR than classic head coils, allowing a higher resolution without loss of information. It does not, however, reduce acquisition time.

To solve the imaging time problem, different reconstruction techniques have been developed [19], and acquisition time is reduced, thanks to a decrease in the number of lines in the *k*-space [20, 21]. Existing methods are sensitivity encoding (SENSE) [22], generalized autocalibrating partially parallel acquisitions (*k-t* GRAPPA) [23], isotropic-voxel radial projection imaging (PC-VIPR) [24], and principal component analysis (PCA), known as *k-t* PCA [25, 26]. Microscopic coils, which are one-element phase-array coils, are not compatible with SENSE for the reconstruction, the latter being restricted to multielement phase-array coils. In contrast, the *k-t* PCA reconstruction method, which reduces data set dimension by exploiting the correlation between data points, is compatible with dS Microscopy coils. The *k-t* PCA method, which generalizes the *k-t* broad-use linear acquisition speed-up technique (BLAST) [27, 28], uses undersampling of the *k-t* space to reduce acquisition time. It was developed by Pedersen et al. [25] to circumvent the issue of peak velocity underestimation of the *k-t* BLAST acceleration [29]. It is based on the PCA method [30], which reduces high-dimensional data into lower dimensions using correlation between data. It considers the image series as a matrix decomposed in a training set and an undersampled set, the *k-t* PCA factor being proportional to the undersampling parameter [29].

The *k-t* PCA technique was evaluated by Knobloch et al. [31] on the carotid bifurcation using a spatial resolution set of $0.8 \times 0.8 \times 0.8$ mm^3 for an acceleration factor set at 8 and an acquisition time of ~ 6 min. They showed that increasing the resolution revealed details of flow patterns hidden at lower spatial resolutions but did not quantify the precision of the measurements. The error was, however, quantified by Giese et al. [32] in the aorta, who showed that *k-t* PCA with an 8-acceleration factor provided acceptable quantitative assessment for the aorta. Nevertheless, the influence of the *k-t* PCA factor has never been tested in millimetric vessels.

The objective now is to determine how to conduct 2D and 4D PC-MRI measurements within millimetric vessels, such as those of the head and face area, with high accuracy and acquisition times compatible with clinical practice. A non-invasive quantification of hemodynamic conditions would, indeed, be of help in choosing recipient vessels in microvascular reconstructions [8] or treat stenoses or arteriovenous malformations [33]. We propose to use a microscopic MRI coil to increase spatial resolution and determine whether the *k-t* PCA technique can be used to decrease acquisition time without compromising its accuracy. Two- and 4D PC-MRI measurements were conducted on two in vitro phantoms with diameters similar to those in the human face and neck area: a Y-bifurcation phantom, the branches of which range from 2 mm to 5 mm in diameter, and a physiological subject-specific phantom of the carotid bifurcation. The same sequences were then applied to in vivo acquisitions of the carotid arterial vasculature for five healthy volunteers: in each case, the internal (ICA), external (ECA) and facial arteries (FA) were acquired. Measurements were compared with 2D PC-MRI acquisitions, which were used as references.

The manuscript is organized as follows: After having explained how the 2D and 4D acquisitions are conducted, we show flow waveforms measured in each branch of the phantoms while increasing the *k-t* PCA acceleration factor systematically. We compare them with flow sensor measurements and conclude by how to optimize acquisition time and accuracy for axial, sagittal, and coronal acquisitions. Precision of the 4D measurements are then determined in the case of in vivo measurements compared with the standard 2D acquisitions. All results are then analyzed to deduce the influence of the *k-t* PCA method and optimal parameters for conducting 4D PC-MRI measurements with clinically relevant scan durations.

Materials and methods

Vessel phantoms

Two Plexiglass in vitro rigid vessel phantomswere used. Phantom 1 is composed of six branches (Fig. 1a): one inlet, one outlet, and four forming a diamond shape. The

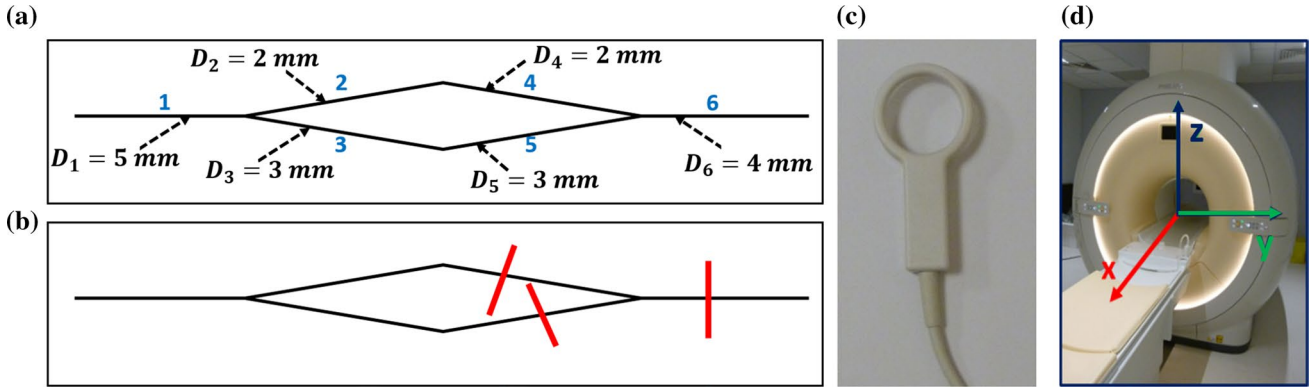

Fig. 1 **a** Geometric characteristics of the in vitro Y-bifurcation phantom (branch numbers indicated in blue). **b** Positioning of the 2D phase-contrast magnetic resonance imaging (PC-MRI) measurement slices within the phantom. **c** dStream (dS) Microscopy coil 47-mm diameter. **d** Orientation of MRI axes

branches are numbered as follows: the inlet channel (branch 1) bifurcates into two sets of V-branches (branches 2–4 and 3–5), which rejoin into a common outlet channel (branch 6). Branch diameters $D_i (i = 1 \ldots 6)$ are, respectively, 5, 2, 3, 2, 3, and 4 mm.

Phantom 2 is an anatomically realistic phantom of a carotid bifurcation and of the vascular tree stemming from the external carotid. Its goal is to show the ability of the present PC-MRI sequences to conduct measurements within clinical conditions. It was obtained through 3D phase-contrast angiography on a 25-year-old healthy man with a 30 cm/s-velocity encoding [34]. The 3D data set of the right carotid bifurcation angiogram was contained within 90 slices of 1.2 mm in thickness and obtained with a spatial resolution of $0.6 \times 0.6\ mm^2$. The Digital Imaging in Communication in Medicine (DICOM) data sets were processed with the ITK-SNAP software [35] to reconstruct the lumen volumes of the vessels, which were exported upon segmentation into a stereolithography file to create the phantom in clear resin (Fig. 2) using a fused-deposition rapid prototyping system. The typical branch diameters are $D_{CCA} = 7$ mm for the common carotid artery, $D_{ICA} = 6$ mm and $D_{ECA} = 5$ mm for the internal and external carotid arteries, $D_{FA} = 2.5$ mm for the facial artery, $D_{LA} = 2$ mm for the lingual artery, and $D_{TSA} = 2.5$ mm for the thyroid superior artery.

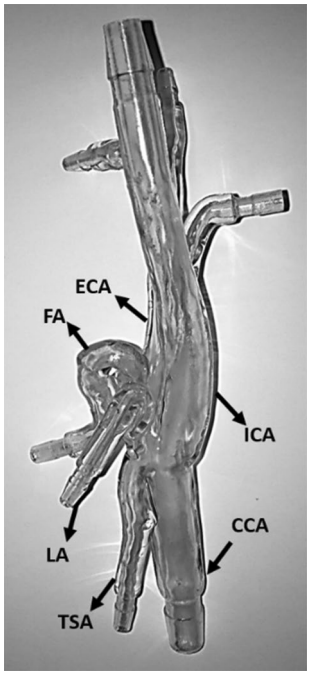

Fig. 2 Physiological subject-specific phantom of the carotid bifurcation. *CCA* common carotid artery, *ICA* internal carotid artery, *ECA* external carotid artery, *FA* facial artery, *LA* lingual artery, *TSA* thyroid superior artery

In vitro experimental setup

The pulsatile flow is provided by a custom-made peristaltic pump (Masterflex), with a frequency of 100 cycles/min and an average flow rate of 85 ml/min. The phantoms are perfused by a Newtonian and incompressible fluid of viscosity 1 mPa.s (pure water). They are connected to the pump by a rigid tube 5 mm in diameter and 10 m in length. The measurements are performed outside the MRI chamber, reproducing the same conditions as those found during MR acquisitions. The dynamic pulse is determined by placing the plethysmograph on a small finger-like compliant tube placed downstream of the phantom, which is used to synchronize MRI acquisitions with the pump frequency. The phantom is placed along the axis of the MRI machine to orient the flow in the same direction as the blood flow in the head and neck arteries of a patient lying down in the MRI. Water gels are placed around the phantom to model tissue and to limit phase errors in MRI measurements. An ultrasonic flow sensor (Transonic System, Inc.) is placed

upstream of the phantoms: repeated flow measurements are acquired to determine the flow waveform with high reproducibility and build the control flow curve (curve named Q_{sensor}).

MRI velocity acquisitions

Veloity fields are acquired using a 3T MR scan (Achieva dStream, Philips) instrument with a dS Microscopy coil 47 mm in diameter (Fig. 1c).

Acquisitions on phantom 1 (simplified vessel-bifurcation model)

A time-of-flight (TOF) measurement is first acquired to create a morphological image and help in slice placement for the 2D PC-MRI acquisitions and volume for 4D acquisitions. TOF acquisition parameters are field of view (FOV) 120×120 mm^2, echo/rotation time (TE/TR) 3/23 ms, spatial resolution 0.35×0.35 mm^2, slice thickness 1.2 mm, two repetitions, resulting in the acquisition of 180 slices in the axial plane covering the entire phantom, for a total scanning time of 90 s. Two-dimensional acquisition slices are then placed along branches 4 and 5 and the outflow channel (branch 6), as indicated in Fig. 1b. The 2D PC-MRI measurements are performed with the following parameters: FOV = 30×30 mm^2, TE/TR 9/16 ms, spatial resolution 0.25×0.25 mm^2, slice thickness 2 mm, 3 repetitions and 32 frames for each cycle. Encoding velocity v_{enc} is set at 35 cm/s for the smaller branch of the bifurcation (branch 4), 45 cm/s for the larger branch (branch 5), and 50 cm/s for the outflow branch (branch 6). The sequence is repeated five times on each branch with a *k-t* PCA acceleration factor (developed by Gyrotools LLC, Zurich) set at 0, 2, 4, 8, and 16, the acceleration factor of 0 corresponding to the case in which no *k-t* PCA is applied. Acquisition times are, respectively, 232, 156, 99, 70, and 55 s when the *k-t* PCA acceleration factor is increased from 0 to 16. Images are reconstructed with the MRecon reconstruction software.

The 4D PC-MRI acquisitions are performed in a predefined volume of the phantom using the following settings: FOV 50×50 mm^2, TE/TR 3/11 ms, spatial resolution 0.65×0.65 mm^2, slice thickness 0.65 mm, with two repetitions, 80 slices for axial acquisitions, and 20 slices for sagittal and coronal ones, and 16 frames for each cycle. Hansen et al. [36] established that 10–20 training profiles (k_z 10–20) are adequate to obtain accurate measurements, and Plein et al. [37] confirmed that 11 training profiles were sufficient to compose the training set. All sequences are thus acquired with the training profile parameters set at [11×6] ($k_y = 6$ and $k_z = 11$).

The 4D protocol is repeated several times to acquire the flow in the axial, coronal, and sagittal planes using the same settings, changing only the number of slices: volume is composed of 20 slices for sagittal and coronal acquisitions and 80 for axial acquisitions. Additional 4D flow measurements are acquired after having changed the spatial orientation of the phantom (i.e., orienting the main flow in the *x*-, *y*- and *z*-directions, Fig. 1d), as well as FOV in the case of axial orientation (FOV increased to 100×100 mm^2).

In all these cases, encoding velocity is set at 50 cm/s in all three spatial directions. As in the 2D PC-MRI protocol, the sequence is repeated changing the *k-t* PCA acceleration factor. In the 4D case, it is set at 0, 2, 4, and 8. It is not possible to select a *k-t* PCA factor of 16 for 4D PC-MRI sequences with the Gyrotools patch used. Acquisitions times are represented in Fig. 3: without acceleration, it takes 40 min to acquire the velocity field in the entire volume for axial measurement and 30 min for coronal and sagittal ones. This is reduced to 6–8 min for a *k-t* factor of 8.

Acquisitions on phantom 2 (realistic model of the facial vascular tree)

A TOF sequence is performed with the same parameters as on phantom 1 to acquire the geometry of the realistic phantom model of the carotid bifurcation (phantom 2). Two-dimensional acquisition slices are then placed on the carotid common artery (v_{enc} = 15 cm/s), internal carotid artery (v_{enc} = 15 cm/s), external carotid artery (v_{enc} = 10 cm/s), facial artery (v_{enc} = 10 cm/s), lingual artery (v_{enc} = 10 cm/s), and thyroid superior artery (v_{enc} = 10 cm/s). The 2D PC-MRI parameters are the same as those used on phantom 1

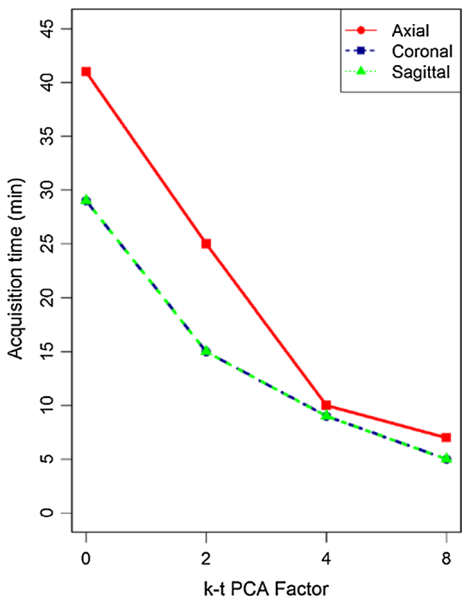

Fig. 3 Acquisition times of the 4D phase-contrast magnetic resonance imaging (PC-MRI) measurements in the axial, coronal, and sagittal directions as a function of the acceleration factor

and no *k-t* PCA acceleration factor is used. Finally, a 4D PC-MRI sequence is performed, covering the entire phantom volume using the same parameters as for phantom 1. The encoding velocity is set at 20 cm/s, *k-t* PCA acceleration factor at 4, and 50 slices are acquired in the axial orientation. The spatiotemporal *k-t* undersampling matrix is reconstructed with the *k-t* PCA method to form the 4D PC-MRI images.

Population for in vivo acquisitions

Five healthy volunteers, one man and four women 22.5 ± 1.4 years old [mean ± standard deviation (SD)], were recruited. The in vivo study was approved by the local ethics committee (No. 2013-A00319-36), registered in clinicaltrials.gov (No. NCT02829190) https://clinicaltrials.gov/ct2/show/NCT02829190?term=NCT02829190&rank=1, and performed in accordance with the ethical standards of the 1964 Declaration of Helsinki. Written informed consent was obtained from all participants.

In vivo acquisitions

The imaging protocol starts with a 3D TOF acquisition, reconstructed in the axial, sagittal, and coronal directions, to provide vessel geometry and help the placement of the 2D slices and 4D volume. The coil is placed at the right side of the face to acquire the right carotid arterial tree and then repeated at the left side. Two planes are successively positioned (Fig. 4) to acquire 2D PC-MRI images with the following parameters: FOV 50 × 50 mm^2, TE/TR 8/13 ms, spatial resolution 0.25 × 0.25 mm^2, slice thickness 2 mm, 32 frames for each cardiac cycle, and a scanning time of ~ 2 min. A first slice allows quantification of the ICA and the ECA with an encoding velocity of 80 cm/s. The second plane is placed orthogonally to the FA with an encoding velocity of 35 cm/s. Then, a 4D PC-MRI volume is placed to acquire the right carotid vasculatures (Fig. 4), and the left carotid vasculature is acquired when the coil is on the left side of the face. To reduce acquisition time of 4D images, the *k-t* PCA method is applied. Parameters of the 4D sequence are: FOV 50 × 50 mm^2, TE/TR 7/12 ms, spatial resolution 0.65 × 0.65 × 0.65 mm^3, *k-t* PCA acceleration factor 4, 16 frames for each cardiac cycle, and a scanning time of ~ 10 min. Acquisition planes are placed in the axial orientation.

Data processing

An internally developed software program, developed on Interactive Data Language (IDL), is used to postprocess phase-contrast MRI images and reconstruct the phantom cross-section in the case of 2D PC-MRI or the phantom inner volume in the case of 4D PC-MRI. The program was originally developed to analyze 2D PC-MRI images [38]. We upgraded it to process 4D PC-MRI images using a semi-automated segmentation based on a fast Fourier transform. We identified voxels contained within the phantom branches by differentiating those varying in synchrony with pump frequency to static ones. After reconstructing the phantom inner volume by 3D segmentation, we selected the cross-cutting planes perpendicular to the branches and analyzed phase intensities of pixels inside the regions of interest (ROI) to reconstruct the waveforms along one cycle. All acquisitions were repeated three times to provide average and SD values.

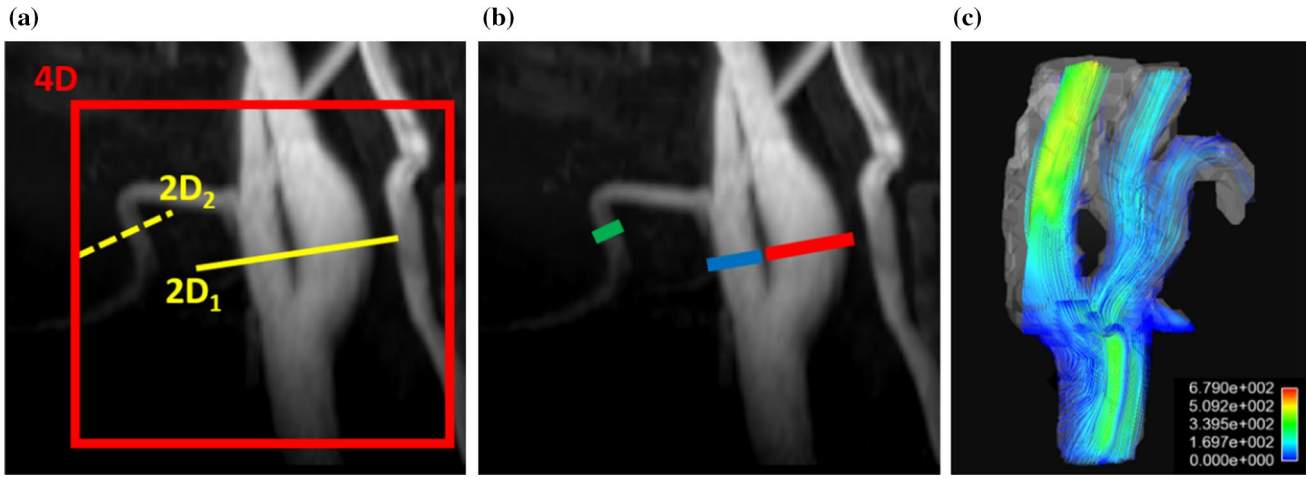

Fig. 4 **a** Positions of 2D slices and 4D volume used for phase-contrast magnetic resonance imaging (PC-MRI) in vivo acquisitions. **b** Aquired arteries: internal carotid artery (red), external carotid (blue), and facial artery (green). **c** Streamline reconstructions from 4D flow measurements with Ensight software

Measurement error ε was determined by calculating the sum of the instantaneous flow rates in branches 4 and 5 (denoted Q_{MRI}), which corresponds to flow rate in the inlet channel, and comparing it to the value Q_{sensor} provided by the flow sensor.

$$\varepsilon = \frac{Q_{\mathrm{MRI}} - Q_{\mathrm{sensor}}}{Q_{\mathrm{sensor}}}. \quad (1)$$

The error is calculated on time-averaged values of the flow rates (denoted $\varepsilon_{\mathrm{mean}}$) and on maximum amplitude of the flow waveform (denoted $\varepsilon_{\mathrm{ampl}}$), which is determined by subtracting the minimum flow rate value from the maximum one for each flow waveform. For the experiment on the physiologically realistic phantom 2, we use 2D PC-MRI acquisitions as reference and calculated acquisition errors of 4D PC-MRI compared with 2D PC-MRI.

Flow waveforms in the ICA, ECA, and FA were extracted from 2D and 4D PC-MRI images. Time-average and peak flow rates were obtained for each vessel, and agreement between 4D and 2D were assessed by Pearson's correlation. Statistical analyses were performed using the R software (version 3.2.2, R Foundation for Statistical Computing, Vienna, Austria, www.r-project.org).

Results

Phantom 1

2D PC-MRI

Figure 5 shows flow waveforms reconstructed from the 2D PC-MRI images and determined from measurements in the bifurcation branches (branches 4 + 5) and the outlet branch (branch 6). Flow curves, obtained for different values of *k-t* PCA acceleration factor, are compared with the control curve (Q_{sensor}). Agreement of MRI measurements with the reference curve was excellent on the whole. Similar values of mean flow rate were found, but a small difference was observable on peak value, which was measured to be slightly higher using MRI than the ultrasonic flow sensor. No characteristic difference in flow profile was, however, found when increasing the *k-t* PCA acceleration factor, regardless of location of the measurement (bifurcation or outlet branches).

Acquisition time was thus divided by a factor 4 when the 16-*k-t* PCA factor is used. Quantitative values of flow rates and measurement errors are indicated in Table 1. Mean flow rates were very consistent, the measurement errors being only a few percent. Slightly larger errors were found on flow amplitude, which corroborates the fact that the error was concentrated on peak flow value, as observed on flow curves (Fig. 5). The error, however, never exceeded 5% and was not influenced by the choice of acceleration factor.

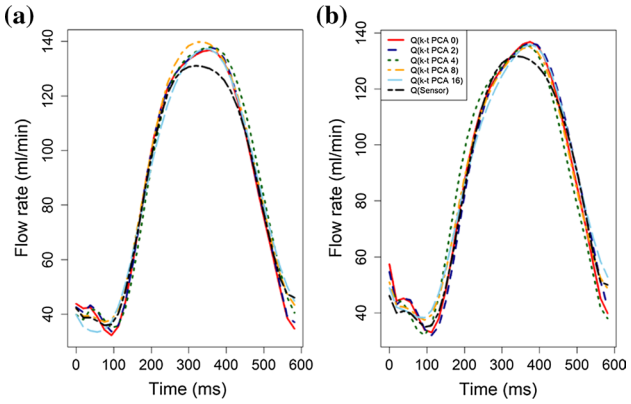

Fig. 5 Flow waveform profiles obtained with 2D phase-contrast magnetic resonance imaging (PC-MRI) sequences for different values of the acceleration factor: **a** Sum of instantaneous flow rates in branches 4 and 5. **b** Instantaneous flow rate in branch 6. MRI flow rates Q_{MRI} are compared with the control curve Q_{sensor} measured by the flow sensor

4D PC-MRI

Flow curves obtained for the different *k-t* PCA acceleration factors in the bifurcation and outlet branches when the phantom is oriented along the *x*-direction are shown in Fig. 6. They correspond to the different acquisition planes: axial, coronal, and sagittal, respectively. Flow curves were compared with the control curve provided by the flow sensor. For axial plane measurements, flow waveform profiles reconstructed from 4D PC-MRI images showed excellent agreement with that provided by the sensor for all *k-t* PCA factors tested. However, for coronal and sagittal plane measurements, only flow waveform profiles acquired with a *k-t* PCA factor set at 0 coincided with the sensor measurement: flow waveform amplitude otherwise strongly decreases as the *k-t* PCA factor increases.

Acquisition time was reduced by a factor of ~ 6 (Fig. 3), and gain in acquisition time was thus even more important than in 2D PC-MRI: this could be due to the smaller number of pixels present per slice in 4D measurements, which speeds up the PCA algorithm.

Figures 7 and 8 show the evolution of measurement errors on mean flow rate and flow amplitude calculated on branches 4 + 5 and the outlet branch as a function of the amplification factor. For measurements in the axial plane, errors remained low for all selected *k-t* PCA factors. The error $\varepsilon_{\mathrm{mean}}$ on the mean flow rate was always < 4% in the bifurcation branches, 7% in the outlet branch, and between 2 and 11% for $\varepsilon_{\mathrm{ampl}}$.

Table 1 Two-dimensional phase-contrast magnetic resonance imaging (PC-MRI) values of acquisition time, mean flow error, and flow amplitude error measured in branches 4 + 5 and 6 of the Y-bifurcation phantom for various values of *k-t* principal component analysis (PCA) factor

k-t PCA factor	0	2	4	8	16
Acquisition time (s)	232	156	99	70	55
Mean flow rate (ml/min) (branches 4–5)	85.4 ± 1.2	86 ± 0.5	86.9 ± 1.8	88.1 ± 2.1	86.1 ± 1.4
Mean flow error ε_{mean} (branches 4–5), (%)	0.5	1.2	2.3	3.7	1.3
Flow amplitude (ml/min) (branches 4–5)	106 ± 3.4	105 ± 3.7	103.5 ± 2.6	102.7 ± 2.6	103.4 ± 4.1
Flow amplitude error ε_{ampl} (branches 4–5), (%)	5	4	2.4	1.7	2.3
Mean flow rate (ml/min) (branch 6)	85.4 ± 0.8	85.7 ± 0.5	85.3 ± 0.4	85.9 ± 1.3	86.8 ± 0.8
Mean flow error ε_{mean} (branch 6) (%)	0.5	0.8	0.4	1.1	2.2
Flow amplitude (ml/min) (branch 6)	104.2 ± 2.2	103.7 ± 1.4	105 ± 1	96.5 ± 3.8	97.3 ± 2.7
Flow amplitude error ε_{ampl} (branch 6), (%)	3.2	2.7	4	4.4	3.7

Much larger errors were, however, obtained for measurements in the coronal and sagittal planes. Errors increased with the *k-t* PCA factor and remained < 14% for ε_{mean}; the amplitude error ε_{ampl} was > 70% in the sagittal plane and ~ 60% in the coronal plane.

To investigate why the errors were larger in the coronal and sagittal planes than in the axial view, when the phantom was oriented in the *x*-direction, we conducted the same measurements orienting the phantom in the *y*- and *z*-directions. Figure 9 shows the corresponding measurement errors on mean flow rate and amplitude. Equivalent results as those shown in Figs. 7 and 8 were obtained when changing the phantom orientation. When the flow direction was in the *z*-direction (*y*-direction, respectively), the error on velocity magnitude was minimal for the coronal plane (sagittal plane, respectively) and significantly larger in the other two directions. These results show the need to align the acquisition direction with the flow direction in the case of 4D measurements when the *k-t* PCA method is used. Without acceleration, there is no constraint on the types of acquisition used.

Another phenomenon that may cause larger measurement errors is the signal itself. To determine its influence, measurements were acquired with a larger FOV (100×100 mm^2) than previously used (phantom oriented along the *x*-direction). Figure 10 compares flow measurement errors in the axial direction with the two FOV sizes. It shows that when no *k-t* PCA is applied, errors are similar whatever the FOV. They do, however, increase faster with the *k-t* PCA factor when the larger FOV is used.

Phantom 2

Flow curves obtained from 2D and 4D PC-MRI acquisitions are displayed in Fig. 11 for measurements within each artery of the physiological subject-specific phantom. Scanning duration times were 3 and 15 min, respectively. Flow waveform profile reconstructed from 4D acquisitions coincide well with those extracted from 2D images. Maximum flow rate had a similar value in both cases. This was confirmed by the difference in values of the 4D versus 2D measurements, as shown in Table 2. The difference was < 7% for all arteries, even in the case of low-flow branches, such as the facial, lingual, and thyroid superior arteries. The time-average flow rate error was, however, more important than the velocity peak error and reached 16% in the facial artery. Error ε_{mean} iwas > 10% for small arteries of the model (external carotid, facial, lingual, and thyroid superior arteries).

In vivo

Figure 12 shows the flow waveform over one cardiac cycle obtained in one volunteer in each artery using 2D and 4D PC-MRI. The 4D flow waveform was smoother than the 2D curve, which was the most notable difference. Another difference was peak flow rate value, which was higher for 2D than for 4D acquisitions. The conclusions are thus the same as in the in vitro case.

Correlations (Fig. 13) for the five healthy volunteers were obtained between 2D (without *k-t* PCA acceleration factor) and 4D (with a *k-t* PCA factor of 4) measurements. The ten vascular trees (5 right + 5 left) were acquired in 2D and 4D using the same methods; Pearson's correlation was performed to compare time-average and peak flow rates. Overall correlations were *r* 0.99 and *r* 0.85 for time-average and peak flow rates, respectively. A poorer correlation was found for peak flow rate, confirming in vitro results.

Discussion

Results of this study show that PC-MRI measurements in millimetric-size vessels with diameters between 2 and 5 mm are possible. They prove the feasibility of reaching voxel sizes of 0.25×0.25 mm^2 in 2D and 0.65×0.65 mm^2 in 4D, with acquisition times compatible with clinical practice.

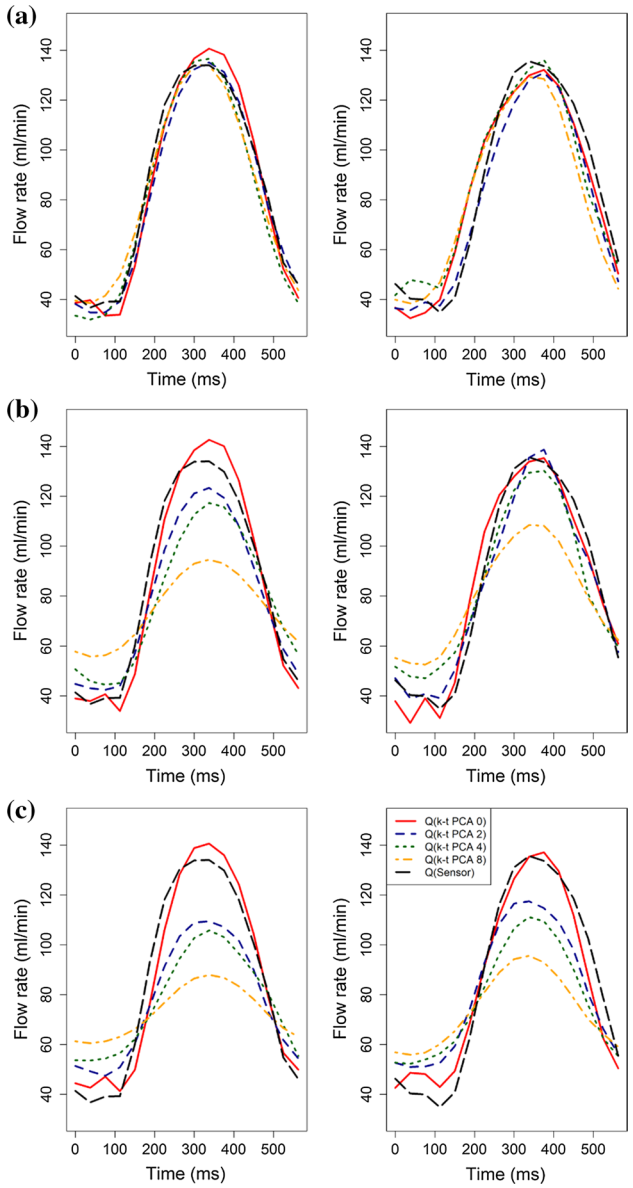

Fig. 6 Flow waveform profiles obtained with the 4D phase-contrast magnetic resonance imaging (PC-MRI) sequences when increasing the acceleration factor from 0 to 8, when the phantom is oriented along the x-direction. Comparison with the control flow rate Q_{sensor} measured by the flow sensor. Measurements are respectively acquired in branches 4 + 5 of the bifurcation (left column) and the outlet branch (right column) in the **a** axial, **b** coronal, and **c** sagittal planes

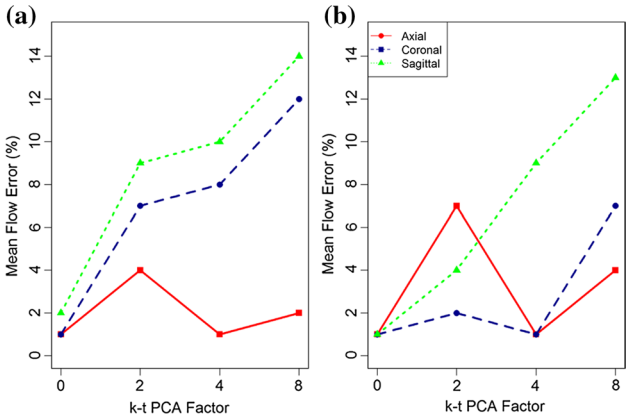

Fig. 7 Mean flow error $\varepsilon_{\text{mean}}$ measured in the axial, coronal, and sagittal planes in **a** bifurcation branches 4 + 5 and **b** the outlet branch as a function of the acceleration factor (phantom oriented along the x-direction)

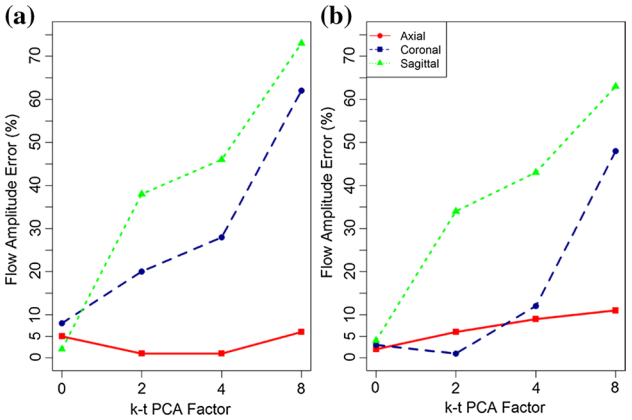

Fig. 8 Flow amplitude error $\varepsilon_{\text{ampl}}$ measured in the axial, coronal, and sagittal planes in **a** bifurcation branches 4 + 5 and **b** outlet branch as a function of the acceleration factor (phantom oriented along the x-direction)

We show that the *k-t* PCA acceleration factor can be applied without any restriction in 2D acquisitions and that *k-t* PCA then allows acquisition time to be divided by a factor of 4, without loss in precision in the measured velocity and flow rate values. It not only preserves the shape of the flow waveform, but mean flow error was always < 4% (maximum error even being obtained when no *k-t* PCA acceleration was used). It is thus possible to apply a *k-t* PCA acceleration factor for flow quantification at high resolution in vessels < 5 mm, which has the advantage of reducing acquisition time significantly without loss of information or precision.

The *k-t* PCA method was originally developed to overcome the issue of loss in amplitude and underestimation of peak velocities found with the *k-t* BLAST reconstruction [29]. The study presented here conducted in subcentimetric vessels shows that the problem is fully solved by the *k-t* PCA method in 2D PC-MRI measurements but only partially in 4D: in this case, only axial acquisitions provide highly accurate flow measurements for a vessel oriented in the axial direction. By changing phantom orientation, the same is true for any other flow/acquisition orientations. A loss in flow amplitude was found in acquisitions in the perpendicular planes (coronal and sagittal in the case of vessel flow in the axial direction), even for a *k-t* PCA acceleration factor as low

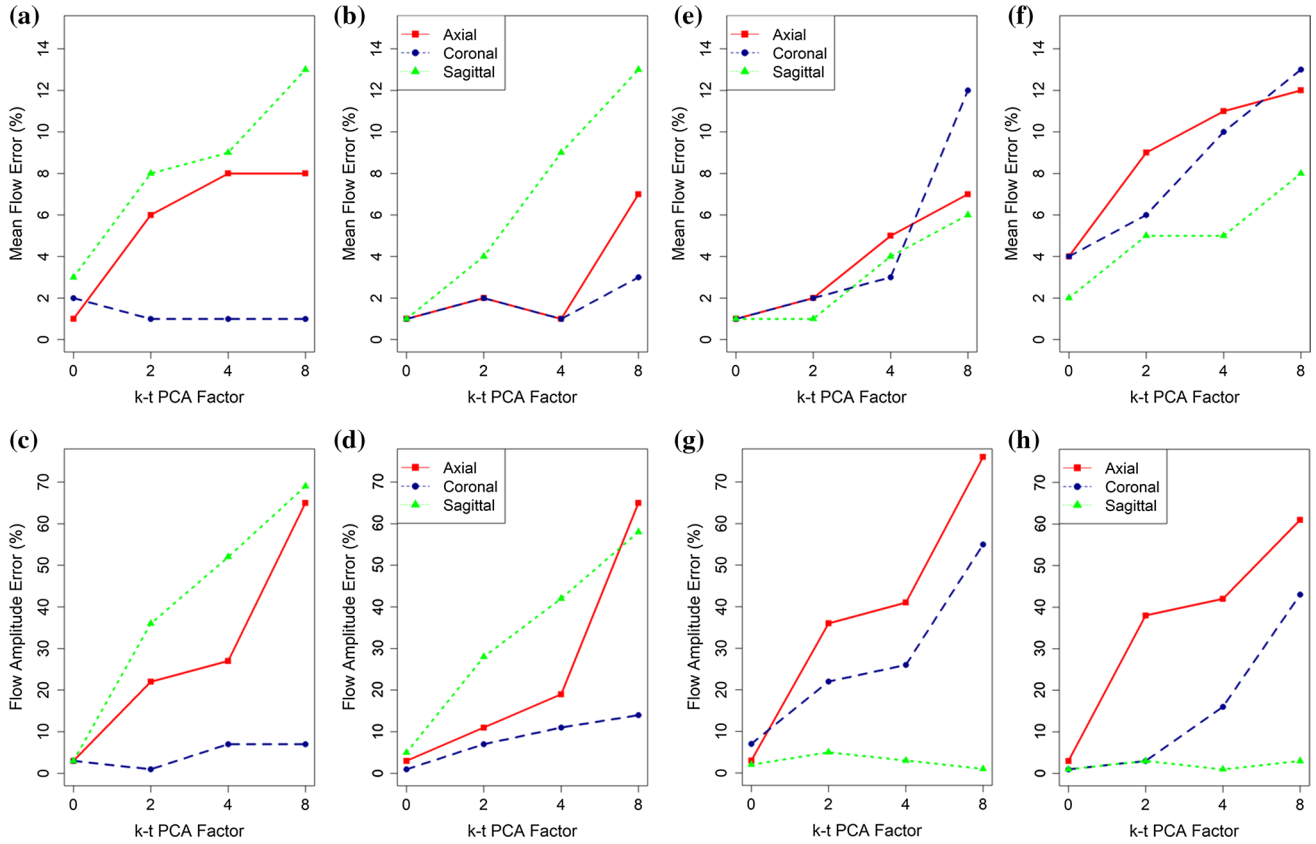

Fig. 9 **a–h** Effect of phantom orientation on errors of flow measurements in the axial, coronal, and sagittal planes as a function of the acceleration factor. Mean flow error ε_{mean} measured in bifurcation branches 4 + 5 (**a**, **e**) and outlet branch (**b**, **f**) when the phantom was oriented in the *z*-/*y*-direction. Flow amplitude error ε_{ampl} measured in bifurcation branches 4 + 5 (**c**, **g**) and outlet branch (**d**, **h**) when the phantom is oriented in *z*-/*y*-direction

as 2. This loss in flow amplitude is not related to the acquisition plane itself, as 4D measurements obtained in the axial, coronal, and sagittal planes perfectly fit one another without *k-t* PCA acceleration factor. This is due to the difficulty of the PCA method to reconstruct the velocity field when the measurement slice is not perpendicular to the flow. This is due to the absence of correlation in the local velocity for many pixels in the cutting plane, which decreases the friability of velocity measurements in these cases.

Results of the parametric study thus confirm the feasibility of applying the *k-t* PCA acceleration factor for acquisitions in the axial plane, even when the maximum value of the acceleration factor (8) is used. Mean flow error ε_{mean} is then < 5% and the flow amplitude error ε_{ampl} < 10%, which is consistent with results of Giese et al. [32] on larger vessels. Increasing the *k-t* PCA acceleration factor causes a slight increase in the amount of information lost (and thus in the flow measurement error), but it reduces the acquisition time significantly. In the case of axial acquisitions, it thus seems appropriate to use an acceleration factor of 8 to reduce the time by a factor of 6.

It is interesting to note that although small, measurement errors increase as the size of the tube is decreased (Table 1). The principal explanation is the decrease in spatial resolution. In small branches, artefacts such as partial volume effects [39] can also cause measurement errors. This effect was similarly observed by Van Ooij et al. [40] in an aneurysm phantom model for 4D flow sequence applied with *k-t* BLAST and SENSE acceleration methods.

Four-dimensional PC-MRI acquisitions in perpendicular directions to blood flow may only be conducted without *k-t* PCA: mean flow error ε_{mean} actually remains < 10% up to an acceleration factor of 4, but the flow amplitude error ε_{ampl} is higher than 10% whenever an acceleration factor is applied. It reaches values well above 50% in both bifurcation and outflow branches for an acceleration set at 8, which is much beyond any acceptable limits. All these results indicate that no *k-t* acceleration factor ought to be used to acquire actual flow waveforms. Giese et al. [32] also found that results in larger vessels differ for coronal and sagittal acquisitions and that the *k-t* PCA method leads to important errors, whatever the value of the acceleration factor.

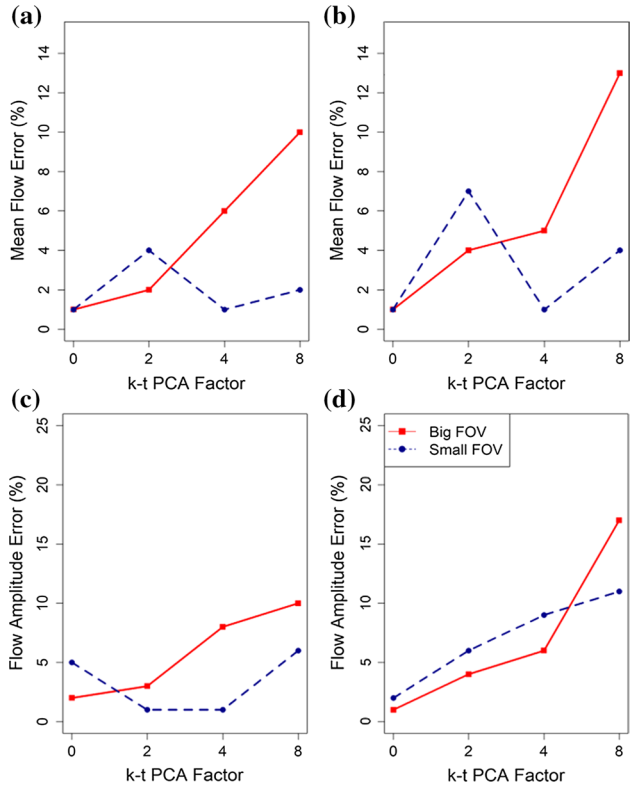

Fig. 10 Effect of field of view (FOV) size on axial flow measurement errors as a function of the acceleration factor: comparison between an FOV of 50 × 50 mm^2 (blue line) and 100 × 100 mm^2 (red line). Mean flow error ε_{mean} in **a** bifurcation branches 4 + 5 and **b** outlet branch. Flow amplitude error ε_{ampl} in the axial planes in **c** bifurcation branches 4 + 5 and **d** outlet branch

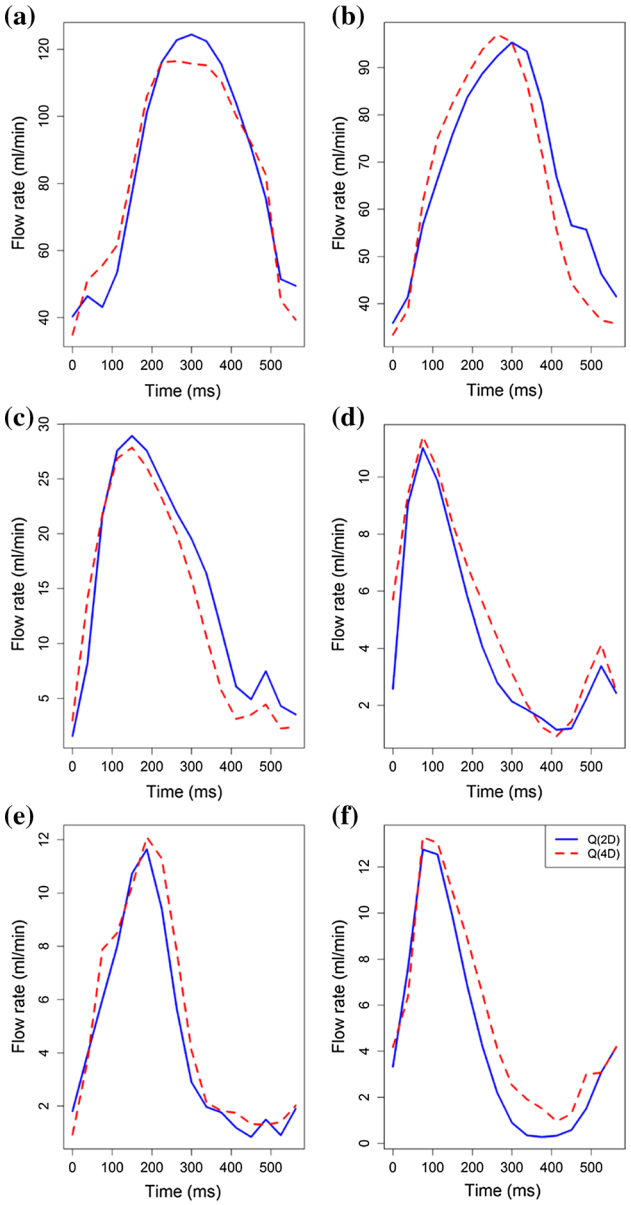

Fig. 11 Flow waveform profiles measured in the physiological subject-specific phantom with the 4D phase-contrast magnetic resonance (PC-MRI) sequences. Comparison with 2D PC-MRI measurements: **a** common carotid artery, **b** internal carotid artery, **c** external carotid artery, **d** facial artery, **e** lingual artery, and **f** thyroid superior artery

The higher error in the sagittal than in the coronal plane can also be explained by the presence of insufficient signal in some slices: this occurs in 11 sagittal but only six coronal slices. Most of these slices are principally composed of noise, which reduces the number of voxels with signal, explaining why the principal component method fails.

Apart from vessel flow direction, a second source of error for the *k-t* PCA method may come from the signal itself. To see the impact of the FOV, we also conducted measurements considering a larger FOV (100 × 100 mm^2) and compared results with the one presently used. When no *k-t* PCA is applied, errors are similar whatever the FOV. However, they increase faster with the *k-t* PCA factor when the larger FOV is used. This can be explained by a weaker flow signal in the case of the larger FOV, which makes it difficult for the algorithm to accurately reconstruct the velocities. The maximum error is, however, of the order of 13% when a *k-t* factor of 8 is used, which is much below the maximum error values of Fig. 8. This shows that the impact of the FOV is of secondary importance compared with the effect of flow direction. In the case of large vessels, such as the aorta, orientation has a limited effect because flow is almost unidirectional, and the vessel has sufficiently large cross-sections for the pixels to be correlated.

The 4D PC-MRI acquisition performed in vivo and on the physiologically realistic phantom confirm that it is possible to apply the *k-t* PCA method to explore blood flow in millimetric vessels with acquisition times of 15 min at maximum. Indeed, very good agreement was found between flow waveform profiles measured with 2D (without use of *k-t* PCA acceleration factor) and in 4D (with a *k-t* PCA factor of 4) flow measurements. Spatial resolution of the sequences

Table 2 Reference values of mean flow rate and flow amplitude measured using 2D phase-contrast magnetic resonance imaging (PC-MRI) in the different branches of the subject-specific phantom (Fig. 2)

Artery	CCA	ICA	ECA	FA	LA	TSA
2D mean flow rate (ml/min)	83.4 ± 1.3	67.5 ± 2.4	17 ± 1.9	4.3 ± 0.8	4.4 ± 1.5	4.4 ± 0.2
4D mean flow rate (ml/min)	84.4 ± 4.3	67.4 ± 5.7	14.2 ± 2	3.6 ± 1.8	3.9 ± 2.7	3.8 ± 1.8
4D mean flow error ϵ_{mean}, (%)	1.2	4.5	16.6	16.3	11.8	13
2D flow amplitude (ml/min)	88.2 ± 2.5	59.2 ± 1.2	28 ± 2.5	11.1 ± 1	12.2 ± 2.2	12.9 ± 1.6
4D flow amplitude (ml/min)	82 ± 5.2	57.8 ± 4.5	26.5 ± 1.1	10.5 ± 2	12.1 ± 2.9	12.1 ± 1.2
4D flow amplitude error ϵ_{ampl}, (%)	7.1	2.3	5.5	6	1.2	5.9

Corresponding values for 4D compared with 2D measurements are indicated below each one (*k-t* PCA acceleration factor of 4)

ICA internal carotid artery, *ECA* external carotid artery, *FA* facial arteries

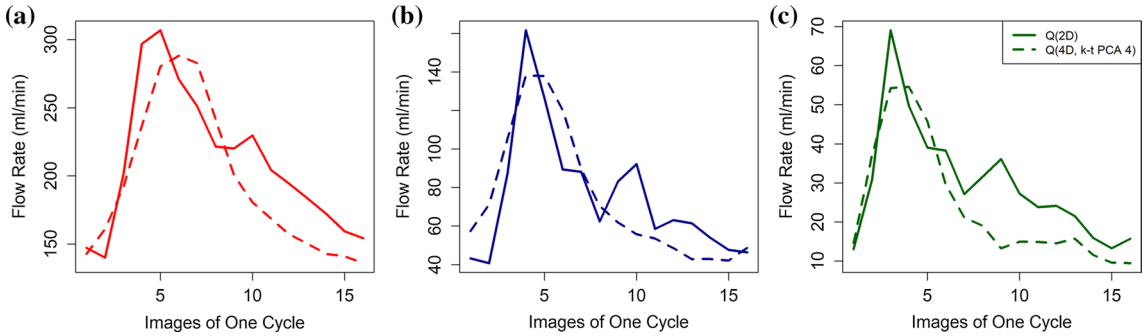

Fig. 12 Comparison of flow profile in the **a** internal carotid artery, **b** external carotid artery, and **c** facial artery measured using 2D and 4D phase-contrast magnetic resonance imaging (PC-MRI)

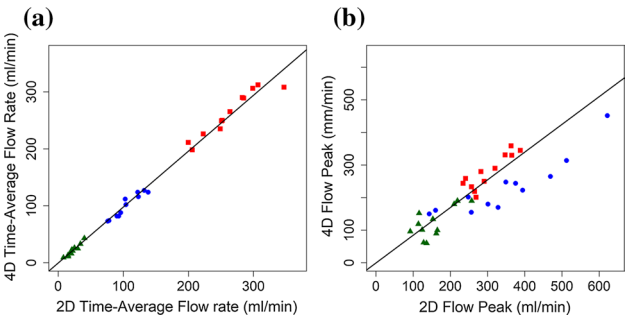

Fig. 13 Pearson's correlation of the comparison of **a** time-average flow rate (r^2 0.99) and **b** peak flow rate (r^2 0.85) measured using 4D and 2D phase-contrast magnetic resonance imaging (PC-MRI)

guarantees good accuracy for flow measurements in vessels characterized by flow rates as small as 4 ml/min and diameters as small as 2 mm. Still, in vivo measurements showed smoothing of the flow curve due to data undersampling. This smoothing effect was not visible on phantom data because the pump provided a "perfect" signal, which did not fully reflect the reality of blood flow.

In the in vitro measurements, a small difference in mean flow rate was observed, especially for the smallest vessels. This can be explained by the higher spatial and temporal resolutions used in 2D than in 4D sequences. The difference can also be attributed to flow-rate value measured in the smallest arteries (~ 5 ml/min): any little variation in flow rate can produce a great percent error between measurements. One must, however, keep in mind that only one encoding velocity can be set in 4D PC-MRI measurements and that it is necessary to select it depending on the maximum flow velocity present in the phantom (or vasculature) to avoid aliasing artefacts. Encoding velocity may, then, not be adapted to small branches (or vessels) and locally cause a loss in signal.

Conclusion

In conclusion, we have proven, using an experimental in vitro setup mimicking physiological pulsatile flow conditions, the possibility of acquiring high-resolution MRI velocity measurements in millimetric vessels. Two- and 4D PC-MRI measurements were performed in vessels < 5 mm with acquisitions time < 10 min per sequence. High precision and small duration times were guaranteed by using a dS Microscopy coil and high *k-t* PCA acceleration factor values. The maximum possible values of the acceleration factor can be used for 2D and of 4D PC-MRI acquisitions as long as

measurements are in the same direction as blood flow in the vessel of interest. No acceleration factor should, however, be used for 4D acquisitions in the directions perpendicular to blood flow, as it causes a decrease in flow curve amplitude. After validating the 4D PC-MRI sequences on the in vitro V-bifurcated phantom, acquisitions of the carotid bifurcation were performed in a realistic model in which some branch were only 2 mm in diameter. They proved that accurate quantitative flow data could be obtained in complex millimetric vasculatures with clinically acceptable acquisition times (< 15 min) with voxel sizes of 0.25×0.25 mm^2 in 2D and 0.65×0.65 mm^2 in 4D. In vivo results confirmed the effect of *k-t* PCA acceleration factor for 4D acquisitions in vasculatures composed of small vessels, such as the facial artery. This finding opens the possibility of conducting a complete biomechanical assessment during surgical planning, whatever the size of the vessel of interest, and to consider geometric as well as hemodynamic information.

Acknowledgements The research was funded in part by the *Région Picardie* (FlowFace Project), by the Foundation Gueules Cassées, and by the French National Research Agency (Grant ANR-10-EQPX-01-01). The authors are grateful to the staff members at the *Institut Faire Faces* (Amiens, France) for technical assistance, and warmly thank Danielle Lembach and Sophie Potier for their participation in the MRI acquisitions.

Author contributions Protocol/project development: GP, JB, A.-VS, OB. Data collection or management: GP, JB, A.-VS. Data analysis: GP, A.-VS.

Compliance with ethical standards

Conflict of interest The authors declare that they have no conflict of interest.

Ethical standards All procedures performed in studies involving human participants were in accordance with the ethical standards of the institutional and/or national research committee and with the 1964 Helsinki declaration and its later amendments or comparable ethical standards.

References

1. Nayler GL, Firmin DN, Longmore DB (1986) Blood flow imaging by cine magnetic resonance. J Comput Assist Tomogr 10(5):715–722
2. Pelc NJ, Herfkens RJ, Shimakawa A, Enzmann DR (1991) Phase contrast cine magnetic resonance imaging. Magn Reson Q 7(4):229–254
3. Wigström L, Sjöqvist L, Wranne B (1996) Temporally resolved 3D phase-contrast imaging. Magn Reson Med 36(5):800–803
4. Markl M, Chan FP, Alley MT, Wedding KL, Draney MT, Elkins CJ, Parker DW, Wicker R, Taylor CA, Herfkens RJ, Pelc NJ (2003) Time-resolved three-dimensional phase-contrast MRI. J Magn Reson Imaging 17(4):499–506
5. Markl M, Kilner PJ, Ebbers T (2011) Comprehensive 4D velocity mapping of the heart and great vessels by cardiovascular magnetic resonance. J Cardiovasc Magn Reson Off J Soc Cardiovasc Magn Reson 13:7
6. Harloff A, Albrecht F, Spreer J, Stalder Af, Bock J, Frydrychowicz A, Schöllhorn J, Hetzel A, Schumacher M, Henning J, Markl M (2009) 3D blood flow characteristics in the carotid artery bifurcation assessed by flow-sensitive 4D MRI at 3T. Magn Reson Med 61(1):65–74
7. Frydrychowicz A, Markl M, Hirtler D, Harloff A, Schlensak C, Geiger J, Stiller B, Arnold R (2011) Aortic hemodynamics in patients with and without repair of aortic coarctation: in vivo analysis by 4D flow-sensitive magnetic resonance imaging. Invest Radiol 46(5):317–325
8. Crook SES, Hope MD (2011) Arch hypoplasia and aneurysm after aortic coarctation repair abnormal flow may be the link. JACC Cardiovasc Imaging 4(6):685–686
9. Af Stalder, Mf Russe, Frydrychowicz A, Bock J, Hennig J, Markl M (2008) Quantitative 2D and 3D phase contrast MRI: optimized analysis of blood flow and vessel wall parameters. Magn Reson Med 60(5):1218–1231
10. Potters WV, van Ooij P, Marquering H, vanBavel E, Nederveen AJ (2015) Volumetric arterial wall shear stress calculation based on cine phase contrast MRI. J Magn Reson Imaging 41(2):505–516
11. Markl M, Wallis W, Brendecke S, Simon J, Frydrychowicz A, Harloff A (2010) Estimation of global aortic pulse wave velocity by flow-sensitive 4D MRI. Magn Reson Med 63(6):1575–1582
12. Wetzel S, Meckel S, Frydrychowicz A, Bonati L, Radue E-W, Scheffler K, Hennig J, Markl M (2007) In vivo assessment and visualization of intracranial arterial hemodynamics with flow-sensitized 4D MR imaging at 3T. Am J Neuroradiol 28(3):433–438
13. Yamashita S, Isoda H, Hirano M, Takeda H, Inagawa S, Takehara Y, Alley MT, Markl M, Pelc NJ, Sakahara H (2007) Visualization of hemodynamics in intracranial arteries using time-resolved three-dimensional phase-contrast MRI. J Magn Reson Imaging 25(3):473–478
14. Bammer R, Hope TA, Aksoy M, Alley MT (2007) Time-resolved 3D quantitative flow MRI of the major intracranial vessels: Initial experience and comparative evaluation at 1.5 T and 3.0 T in combination with parallel imaging. Magn Reson Med 57(1):127–140
15. Frydrychowicz A, Francois CJ, Turski PA (2011) Four-dimensional phase contrast magnetic resonance angiography: potential clinical applications. Eur J Radiol 80(1):24–35
16. Cibis M, Potters WV, Gijsen FJH, Marquering H, vanBavel E, van der Steen AFW, Nederveen AJ, Wentzel JJ (2014) Wall shear stress calculations based on 3D cine phase contrast MRI and computational fluid dynamics: a comparison study in healthy carotid arteries. NMR Biomed 27(7):826–834
17. Harloff A, Zech T, Wegent F, Strecker C, Weiller C, Markl M (2013) Comparison of blood flow velocity quantification by 4D flow MR imaging with ultrasound at the carotid bifurcation. Am J Neuroradiol 34(7):1407–1413
18. Markl M, Wegent F, Zech T, Bauer S, Strecker C, Schumacher M, Weiller C, Hennig J, Harloff A (2010) In vivo wall shear stress distribution in the carotid artery effect of bifurcation geometry, internal carotid artery stenosis, and recanalization therapy. Circ Cardiovasc Imaging 3(6):647–655
19. Christodoulou AG, Zhang H, Zhao B, Hitchens TK, Ho C, Liang ZP (2013) High-resolution cardiovascular MRI by integrating parallel imaging with low-rank and sparse modeling. IEEE Trans Biomed Eng 60(11):3083–3092
20. Pruessmann KP (2006) Encoding and reconstruction in parallel MRI. NMR Biomed 19(3):288–299
21. Jung B, Honal M, Ullmann P, Hennig J, Markl M (2008) Highly k-t-space–accelerated phase-contrast MRI. Magn Reson Med 60(5):1169–1177

22. Pruessmann KP, Weiger M, Scheidegger MB, Boesiger P (1999) SENSE: sensitivity encoding for fast MRI. Magn Reson Med 42(5):952–962
23. Jung B, Stalder AF, Bauer S, Markl M (2011) On the undersampling strategies to accelerate time-resolved 3D imaging using k-t-GRAPPA. Magn Reson Med 66(4):966–975
24. Gu T, Korosec FR, Block WF, Fain SB, Turk Q, Lum D, Zhou Y, Grist TM, Haughton V, Mistretta C (2005) PC VIPR: a high-speed 3D phase-contrast method for flow quantification and high-resolution angiography. Am J Neuroradiol 26(4):743–749
25. Pedersen H, Kozerke S, Ringgaard S, Nehrke K, Kim WY (2009) k-t PCA: temporally constrained *k-t* BLAST reconstruction using principal component analysis. Magn Reson Med 62(3):706–716
26. Vitanis V, Manka R, Giese D, Pedersen H, Plein S, Boesiger P, Kozerke S (2011) High resolution three-dimensional cardiac perfusion imaging using compartment-based *k-t* principal component analysis. Magn Reson Med 65(2):575–587
27. Tsao J, Boesiger P, Pruessmann KP (2003) *k-t* BLAST and *k-t* SENSE: dynamic MRI with high frame rate exploiting spatiotemporal correlations. Magn Reson Med 50(5):1031–1042
28. Kozerke S, Tsao J, Razavi R, Boesiger P (2004) Accelerating cardiac cine 3D imaging using *k-t* BLAST. Magn Reson Med 52(1):19–26
29. Stadlbauer A, van der Riet W, Crelier G, Salomonowitz E (2010) Accelerated time-resolved three-dimensional MR velocity mapping of blood flow patterns in the aorta using SENSE and *k-t* BLAST. Eur J Radiol 75(1):e15–e21
30. Pearson K (1901) On lines and planes of closest fit to system of points in space. Philos Mag 2:559–572
31. Knobloch V, Boesiger P, Kozerke S (2013) Sparsity transform k-t principal component analysis for accelerating cine three-dimensional flow measurements. Magn Reson Med 70(1):53–63
32. Giese D, Schaeffter T, Kozerke S (2013) Highly undersampled phase-contrast flow measurements using compartment-based k-t principal component analysis. Magn Reson Med 69(2):434–443
33. Marks MP, Pelc NJ, Ross MR, Enzmann DR (1992) Determination of cerebral blood flow with a phase-contrast cine MR imaging technique: evaluation of normal subjects and patients with arteriovenous malformations. Radiology 182(2):467–476
34. Bettoni JB, Pagé G, Dakpé S, Balédent O (2015) MRI flow quantification of head and neck flow arteries. In: Proceedings of the 32th scientific meeting, European Society for Magnetic Resonance in Medicine and Biology, Edimburg, p 128
35. Yushkevich PA, Piven J, Hazlett HC, Smith RG, Ho S, Gee JC, Gerig G (2006) User-guided 3D active contour segmentation of anatomical structures: significantly improved efficiency and reliability. NeuroImage 31(3):1116–1128
36. Hansen MS, Kozerke S, Pruessmann KP, Boesiger P, Pedersen EM, Tsao J (2004) On the influence of training data quality in k-t BLAST reconstruction. Magn Reson Med 52(5):1175–1183
37. Plein S, Ryf S, Schwitter J, Radjenovic A, Boesiger P, Kozerke S (2007) Dynamic contrast-enhanced myocardial perfusion MRI accelerated with k-t sense. Magn Reson Med 58(4):777–785
38. Balédent O, Henry-Feugeas MC, Idy-Peretti I (2001) Cerebrospinal fluid dynamics and relation with blood flow: a magnetic resonance study with semiautomated cerebrospinal fluid segmentation. Invest Radiol 36(7):368–377
39. Pelc NJ, Sommer FG, Brosnan TJ, Herfkens RJ, Enzman DR (1994) Quantitative magnetic resonance flow imaging. Magn Reson Q 10(3):125–147
40. van Ooij P, Guédon A, Marquering H, Schneiders J, Majoie C, van Bavel E, Nederveen AJ (2013) k-t BLAST and SENSE accelerated time-resolved three-dimensional phase contrast MRI in an intracranial aneurysm. Magn Reson Mater Phy. 26(3):261–270